

This discussion paper is/has been under review for the journal Biogeosciences (BG).
Please refer to the corresponding final paper in BG if available.

A two-dimensional model of the passive coastal margin deep sedimentary carbon and methane cycles

D. E. Archer¹, B. A. Buffett², and P. C. McGuire¹

¹Department of the Geophysical Sciences, University of Chicago, USA

²Department of Earth and Planetary Sciences, University of California, Berkeley, USA

Received: 28 February 2012 – Accepted: 29 February 2012 – Published: 14 March 2012

Correspondence to: D. E. Archer (d-archer@uchicago.edu)

Published by Copernicus Publications on behalf of the European Geosciences Union.

BGD

9, 2921–2966, 2012

**Passive coastal
margin deep
sedimentary carbon
and methane cycles**

D. E. Archer et al.

Title Page

Abstract

Introduction

Conclusions

References

Tables

Figures

⏪

⏩

◀

▶

Back

Close

Full Screen / Esc

Printer-friendly Version

Interactive Discussion

Abstract

We present a new geologic-time and basin-spatial scale model of the continental margin methane cycle. The model, SpongeBOB, is used to simulate evolution of the carbon cycle in a passive sedimentary continental margin in response to changing oceanographic and geologic forcing over a time scale of 140 million years. The model is somewhat less sensitive to temperature than our previous results with a one-dimensional model, but is more sensitive to reasonable changes in POC than it is to reasonable changes in temperature. This behavior could lead to higher inventories of hydrate during hothouse climate conditions, rather than lower as generally assumed, due to the enrichment of the sediments in organic carbon. The hydrate inventory in the model is extremely sensitive to the ability of methane bubbles to rise within the sediment column, and how far gas-phase methane can get through the sediment column before it redissolves when it reaches undersaturated conditions. Hydrate formation is also sensitive to deep respiration of migrating petroleum in the model. The geochemistry of the sediment column is altered by the addition of vertical high-permeability chimneys intended to mimic the effects of heterogeneity in the real sediment column due to faults and chimneys, and produces results consistent with measured pore-water tracers SO_4^{2-} and ^{129}I . Pore water DIC concentrations are consistent with chemical weathering at depth within the sediment column. The carbon isotopic composition of the DIC is consistent with a methane production efficiency from POC of 50 %, which is somewhat lower than redox balance with the H/C of organic matter in the model. Other phenomena which we simulated had only small impact on the hydrate inventory, including thermogenic methane, dissolved organic carbon, and sediment transport characteristics.

1 Introduction

Models of methane hydrate formation in sediments of the deep-sea have tended to follow the example of early diagenesis modeling in adopting a one-dimensional formu-

BGD

9, 2921–2966, 2012

Passive coastal margin deep sedimentary carbon and methane cycles

D. E. Archer et al.

Title Page

Abstract

Introduction

Conclusions

References

Tables

Figures

⏪

⏩

◀

▶

Back

Close

Full Screen / Esc

Printer-friendly Version

Interactive Discussion



Passive coastal margin deep sedimentary carbon and methane cycles

D. E. Archer et al.

Title Page

Abstract

Introduction

Conclusions

References

Tables

Figures

⏪

⏩

◀

▶

Back

Close

Full Screen / Esc

Printer-friendly Version

Interactive Discussion

lation (Davie and Buffett, 2001; Davie and Buffett, 2003a; Davie and Buffett, 2003b). For the top meter of the sediment column (Archer et al., 2002), the 1-D approximation is a good one, because vertical diffusion is far faster than any possible lateral pore fluid transport or diffusional effects. The methane cycle challenges a 1-D formulation, however, because the relevant chemical processes occur hundreds of meters below the sea floor, and clearly show the impact of pore fluid and gas phase migration in more than one dimension. One-dimensional models of the upper sediment require fluid flow imposed as a bottom boundary condition, and the hydrate inventory of the model is very sensitive to this parameter (Buffett and Archer, 2004). The methane cycle is also impacted by time-dependence of the sediment and organic carbon deposition rates, which are governed by onshore-offshore processes, another benefit of incorporating the second dimension into the model formulation.

SpongeBOB is formulated in the onshore-offshore dimension laterally, and to bedrock in the vertical, to internalize the entire coastal margin carbon and methane cycle, of which the methane hydrates near the sea floor are just one manifestation. Many of the processes and mechanisms, such as all the different means of downslope sediment transport, or pathways for subsurface fluid flow, are impossible to represent accurately given our present state of knowledge, but by representing them as best we are able, we hope to gain some qualitative picture of the relative importances of the various driving factors and processes.

The model is set up to simulate an accumulating passive continental margin such as the East coast of the United States, which has been accumulating sediment since rifting of the Atlantic about 200 million years ago. One of the best-studied locations for methane hydrates is the Blake Ridge, a “drift deposit” ridge jutting out into the Atlantic (Borowski, 2004). The Blake Ridge owes its existence to the hydrodynamics of particle sedimentation, presumably driven by existing topography and the energetic western boundary flow of the Atlantic. Although Blake Ridge is attached to the continental slope of the US, our model results (which only represent the slope, with no drift-deposit ridge)

suggest that Blake Ridge might not be entirely typical of slope sediments in general, and thus might be deceptive jumping-off point for global extrapolation.

We gauge the sensitivities of this complex model by showing a variety of sensitivity model runs, varying critical parameters or turning process on and off. The characteristics of the runs will be described as they come up in the model formulation section, and they are summarized in Tables 1 and 2.

2 Model formulation

2.1 Computational grid

SpongeBOB is formulated on a free-form grid sigma-type vertical coordinate system in depth (Fig. 1), in which the grid cells expand to fill the sediment column as it expands through time. The grid cell thicknesses are controlled through the simulation by the bookkeeping strategy of advecting sediment (solid plus associated pore fluid and other phases) through the interior of the model domain. Initially all grid cells contain enough solid material to fill a thickness of 1 meter at a “drained” porosity. Sediment is deposited on the top face of the top cell, and a material flow rate is calculated for the bottom face of the cell, such that the cell keeps some of the new material for itself, but passes most of it on fill the subsurface cells. The process continues through the sediment column, and the boxes all expand uniformly.

A few grid cells in the top of the domain are restricted, such that they cannot expand beyond a thickness of 200 m, in order to maintain a minimum computational resolution in the region of the hydrate stability zone. After enough model time has passed that a restricted cell reaches its maximum thickness, it passes along the entire incoming advective flux from above into the cell below.

BGD

9, 2921–2966, 2012

Passive coastal margin deep sedimentary carbon and methane cycles

D. E. Archer et al.

Title Page

Abstract

Introduction

Conclusions

References

Tables

Figures

⏪

⏩

◀

▶

Back

Close

Full Screen / Esc

Printer-friendly Version

Interactive Discussion

2.2 Isostasy

The sediment column elevation is determined by a time-dependent, laterally smoothed isostasy calculation, based on the idea that the crust and all the material sitting on top of it are all floating in a denser fluid of mantle material. The model domain spans between continental crust and ocean crust, with a stipulation that only the ocean crust is affected by a time-dependent cooling.

The continental crust is 13 km thick and its density is 3.0 g cm^{-3} . Any sediment load also contributes to the mass of the column, and the equilibrium elevation of the bedrock. Cooling of the ocean crust takes place with a time-dependent thermal boundary layer, in which temperature varies linearly with depth, and the thickness of which increases according to $dz = \sqrt{\kappa T}$ (Parson and Sclater, 1977). The temperatures of the ocean crust and the mantle boundary layer are found by interpolation between the time-evolving temperature at the base of the sediment column, and a generic mantle temperature of 1600°C . A temperature of 1600 K would have been more realistic, but the impact of this coding error on the buoyancy of the crust is small. The ocean end-member sediment column is taken as the sum of the sediment column, the ocean crust, and the thermal boundary layer as it thickens and thermally contracts through time.

The blending of domains is done by calculating pure end-member continental and ocean crust scenarios at each model grid point, and then scaling between them using an ad-hoc ocean fraction variable, ranging from 0 for continent to 1 for the ocean end member. The transition is set up with a horizontal length scale of 50 km. For each end member, continental and oceanic, the masses and heights of the column are computed. The two scenarios are blended together at this stage, taking a composite column mass that scales between the two end members, and a composite column height.

The position of local isostatic equilibrium is determined by mass displacement of generic mantle material, taking a hypothetical mantle “water line” defined such that the nominal elevation of the top of a generic ocean crust falls at about 4000 m below sea

BGD

9, 2921–2966, 2012

Passive coastal margin deep sedimentary carbon and methane cycles

D. E. Archer et al.

Title Page

Abstract

Introduction

Conclusions

References

Tables

Figures

⏪

⏩

◀

▶

Back

Close

Full Screen / Esc

Printer-friendly Version

Interactive Discussion



level. The equilibrium heights for the top of bedrock are smoothed horizontally through the grid using a diffusion algorithm that achieves a spatial scale of a few 10's of kilometers. Flexure and rigidity of the plates becomes important in accretionary margins, but for this study the lateral interaction in isostasy is rudimentary, merely setting the stage for the sediment column.

2.3 Sediment dynamics

2.3.1 Deposition

The goals of the sedimentation scheme are to create appropriate sedimentation rates and grain sizes, in adaptive response to a time-evolving submarine landscape. The existence of a shelf break, and the prograding clinoform pattern of sediment deposition, requires the existence of a region of fast sediment accumulation just off the shelf break, a sediment depocenter. Sediment input from the continent is also sorted by grain size, with largest grains depositing closer to shore and finer grain sediments offshore (Fig. 2).

Offshore sediment transport and deposition in SpongeBOB is parameterized in an approach following Pirmez et al. (1998). The ocean margin is treated as a giant river carrying suspended particles from continental runoff, from left to right in our configuration. As the water depth increases, the flow velocity decreases as a plug flow. Suspended particles settle out following Stokes' law according to their grain size. Particles deposit only if the shear stress at the bed, calculated from the hypothetical river velocity multiplied by a fudge factor, is too slow to lift the particles faster than they sink. The critical shear velocity depends on particle radius, as does the settling speed, effectively sorting the particles by size with offshore distance.

2.3.2 Slope-driven offshore transport

Turbidites in abyssal sediments attest to the importance of slope failure to the margin sediment dynamics. These processes are handled as a function of the sea floor grade.

BGD

9, 2921–2966, 2012

Passive coastal margin deep sedimentary carbon and methane cycles

D. E. Archer et al.

Title Page

Abstract

Introduction

Conclusions

References

Tables

Figures



Back

Close

Full Screen / Esc

Printer-friendly Version

Interactive Discussion



Passive coastal margin deep sedimentary carbon and methane cyclesD. E. Archer et al.

[Title Page](#)[Abstract](#)[Introduction](#)[Conclusions](#)[References](#)[Tables](#)[Figures](#)[Back](#)[Close](#)[Full Screen / Esc](#)[Printer-friendly Version](#)[Interactive Discussion](#)

If the grade exceeds a critical value, here taken to be 6%, the material that would deposit according to the shear/sinking speed criterion is instead classified as “resuspended”. Also, if the sea floor slope ever manages to exceed the critical slope, surface sediment is eroded into the resuspended pool. The resuspended material redeposits using the same settling speed/offshore transport criterion as used for the primary settling material, but resuspended material only begins to deposit where the sea floor slope is less than 1%, reflecting the difference between a turbidity flow which only stops on the plain as opposed to individual sinking particles assumed in the primary sedimenting material (Meiburg and Kneller, 2010).

When material is resuspended, its POC concentration is specified as a function of the water depth at the point of its initial potential deposition. Because the offshore transport is assumed to be turbidites, we assume it escapes the degradation that individual settling particles, the primary deposition, are subject to (in other words, the POC fraction of sedimenting material is specified in the code as a function of depth of original deposition, not redeposition). Resuspended organic carbon is assumed to be distributed among the grain size fractions of the resuspended material according to surface area, selectively concentrated (according to mass) the organic carbon into the smaller size fractions.

The sediment transport scheme is intended to be a utilitarian parameterization of sediment transport processes, rather than a mechanism-resolving model such as Sedflux (Syvitski and Hutton, 2001). The scheme as we have tuned it achieves the goal of a well-defined shelf break, driven by a strong sediment depocenter just off the shelf break, and response to sea level changes that mimics the Sedpak model (Strobel et al., 2003). The accumulation rate at 2 km depth in the model is close to that of Blake Ridge, about 2 cm kyr⁻¹. Total sediment thicknesses and extents are comparable with a seismic images of the Atlantic margin from Kennett (1982) (Fig. 3). Model sensitivity to these sediment transport processes was gauged by altering the critical sea floor slope in sensitivity simulation Lo Slope.

2.3.3 Sea level changes

Sedimentation is heavily impacted by eustatic changes in sea level, with highest rates close to shore but in water that not too shallow. Sea level changes are imposed on the simulation as a 160 million-year cycle, peaking at high sea level in the middle of the simulation and dropping the final 20–30 million years (Fig. 4) (Haq et al., 1987). Two sets of simulations were done, one which neglected time-dependent sea level and POC rain forcing (Table 1), and another set which included these effects (Table 2). Results in this paper will be presented as time slices from various points in the simulations, but animations of the entire runs are available as links from the figure captions.

2.4 Pore fluid flow

2.4.1 Porosity and excess pressure

Fluid flow follows Darcy's law in response to the pore fluid excess pressure gradient (Athy, 1930). The pressure formulation of the model is based on a constitutive equation in which the excess pore fluid pressure can be calculated from the porosity and the mass load overhead (Flemings et al., 2002). The idea is that there is a one-to-one relationship between the porosity of the sediment and the amount of solid load it can support, akin to a bulk compressibility. We find that to fit the entire sediment column requires a double exponential decay, in effect two β values, analogous to two springs of different weights and lengths connected in serial. Coefficient β_1 represents ductile flows and recrystallization of mineral grains, on a depth scale of about 10 km, while β_2 represents the collapse of clays that occurs on a depth scale of about 2 km (Fig. 5),

$$\phi = 0.38 e^{-0.0312 S_{\text{supp}}} + 0.32 e^{-0.2 S_{\text{supp}}}$$

where S_{supp} is the supported solid load. Because of the double exponential form of the constitutive equation, this is an iterative calculation.

BGD

9, 2921–2966, 2012

Passive coastal margin deep sedimentary carbon and methane cycles

D. E. Archer et al.

Title Page

Abstract

Introduction

Conclusions

References

Tables

Figures

⏪

⏩

◀

▶

Back

Close

Full Screen / Esc

Printer-friendly Version

Interactive Discussion



Passive coastal margin deep sedimentary carbon and methane cycles

D. E. Archer et al.

Title Page

Abstract

Introduction

Conclusions

References

Tables

Figures

⏪

⏩

◀

▶

Back

Close

Full Screen / Esc

Printer-friendly Version

Interactive Discussion



The excess pressure, which drives the Darcy flow, is calculated as

$$P_{\text{excess}} = S_v - P_{\text{hydro}} - S_{\text{supp}}$$

where S_v is the total load of the sediment column from all phases, and P_{hydro} is the hydrostatic pressure (the load due to the fluid phase).

2.4.2 Permeability

The permeability k in the vertical direction is parameterized as

$$k = \frac{\bar{r}^2 \phi^{-3}}{180(1 - \phi)}$$

where \bar{r} is the mean grain radius and ϕ the porosity. A factor of 100 anisotropy is imposed (Daigle and Dugan, 2011), such that the permeability along the horizontal grid is 100 times higher than the vertical permeability, to parameterize for the effect of layers like sandy turbidites, that are unresolved in the model.

We show results of two model permeability formulations, one as presented so far, and the other with added vertical chimneys of enhanced permeability, such as faults, pipes, chimneys, and similar structures (cases No Chimneys and Base, respectively). The chimneys are situated every 5 grid cells throughout the model domain, and remain stationary as the continental margin progrades offshore through the simulation. The chimneys are meant to suggest the impact of faults and heterogeneities in the sediment column. The horizontal grid spacing is 3.15 km, the vertical permeability in the chimney is 10 times higher than given above. This is only a crude representation of a realistic flow regime through faults and permeable chimneys which seem to dominate subsurface flows (Flemings et al., 2003). The intent is to gauge in a qualitative way the sense and potential magnitude of the impact of heterogeneity on the flow and chemical evolution of the sediment column.

The permeabilities and the excess pressures of the two simulations at the end of the simulations are shown in Fig. 6.

2.4.3 Darcy flow

The excess pressures drive flow following Darcy's law

$$\phi w_{\text{Darcy}} = \frac{k}{\mu} \Delta P_{\text{excess}}$$

where w_{Darcy} is the Darcy velocity, k is the permeability, μ the interstitial fluid viscosity, ϕ the porosity, and P_{excess} is the pressure in excess of hydrostatic in the pore fluid. The fluid velocity is defined here relative to the solid grains, but the solids also move from one grid cell to another vertically as the vertical grid in the model stretches to fill the expanding sediment column. The vertical motion of pore fluid within the numerical grid is taken as the sum of the Darcy flow plus the "accounting" flow to accommodate the stretching coordinate system

$$w_{\text{bur}} = w_{\text{Darcy}} - \text{Burial}_{\text{fluid}}$$

where w_{bur} , like w_{Darcy} , is defined as relative to the moving cell faces of the numerical grid.

A flow limiter in the vertical protects the calculation from numerically overstepping, for thin, permeable layers, by testing for the change in fluid pressure that would result from unimpeded Darcy flow each time step. If the pressure change exceeds a threshold, a stand-in vertical velocity is calculated that generates a prescribed, limited change in the pressure gradient (and hence also the porosity). The idea is that a thin sandy layer would quickly drain, reaching zero excess pressure gradient, and the velocity is designed to achieve that end in a stable way even if the time step for Darcy flow would need to be much shorter. Most of the vertical flow in the model however is well-resolved in time, leaving the flow limiter for a few "emergency" grid points and times.

2.4.4 Vertical flow relative to the seafloor

Formation of methane hydrate in 1-D models is very sensitive to upward vertical flow of pore fluid carrying methane into the stability zone. A measure for the net vertical flow

BGD

9, 2921–2966, 2012

Passive coastal margin deep sedimentary carbon and methane cycles

D. E. Archer et al.

Title Page

Abstract

Introduction

Conclusions

References

Tables

Figures

⏪

⏩

◀

▶

Back

Close

Full Screen / Esc

Printer-friendly Version

Interactive Discussion



is the fluid flow rate relative to the moving sediment water interface, defined throughout the sediment column as

$$w_{\text{seafloor}} = w_{\text{bur}} + \frac{d}{dt}(z - z_{\text{seafloor}})$$

Like w_{bur} and w_{Darcy} , w_{seafloor} is defined on the cell faces, but at any moment in time the subsurface w_{seafloor} velocities are defined as relative to the moving sea floor, so that if a subsurface parcel were flowing upward just quickly enough to remain at a constant depth below the seafloor, its w_{seafloor} would be defined as zero. Sections of w_{Darcy} and w_{seafloor} are shown in Fig. 7, and values at the sediment surface in Fig. 8.

When vertical permeable chimneys are added to the simulation, the chimneys take most of the compaction flow. The horizontal anisotropy applied to the permeability allows the sediment columns in between the chimneys to vent fluid into the chimneys for expulsion. Interestingly for the formation of methane hydrate discussion to come, the chimneyed simulation finds strongly downward w_{seafloor} in the grid cells in between the chimneys. These cells have vented their upward Darcy flow into the permeable chimneys, leaving the burial flux of fluid with sedimentation to drive w_{seafloor} in the downward direction, where it brings fluid from above into the hydrate stability zone, rather than fluid from below.

2.5 Carbon cycle

2.5.1 Deposition

The carbon cycle of the deep biosphere is driven by the rain of particulate organic carbon (POC) to the sea floor, which depends on changes in sea level. The model encodes a generalization that periods of high sea level generally have enhanced carbon preservation due to low oxygen in the ocean, the Cretaceous being an important example (Hunt et al., 1995). The POC concentration and H/C and O/C ratios of the depositing organic matter depend on water depth and the oxygen state of the ocean (Fig. 4). The

BGD

9, 2921–2966, 2012

Passive coastal margin deep sedimentary carbon and methane cycles

D. E. Archer et al.

Title Page

Abstract

Introduction

Conclusions

References

Tables

Figures

⏪

⏩

◀

▶

Back

Close

Full Screen / Esc

Printer-friendly Version

Interactive Discussion



Passive coastal margin deep sedimentary carbon and methane cycles

D. E. Archer et al.

Title Page

Abstract

Introduction

Conclusions

References

Tables

Figures

⏪

⏩

◀

▶

Back

Close

Full Screen / Esc

Printer-friendly Version

Interactive Discussion

low sea-level ocean, with an oxygen minimum zone but no anoxia, deposits at most 2% dry weight POC, with an H/C ratio of 0.7. The high-sea-level ocean, considered anoxic in the end member, buries up to 5% POC, with an H/C ratio of 2. The POC concentrations are specified as a function of water depth for each ocean state (1 to 4, with 1 being fully oxic and 4 anoxic), and interpolated between ocean states so that carbon deposition can vary smoothly in time, in synchrony with changes in eustatic sea level. The “Atlantic” POC profile is comparable to sediment surface POC concentration off Cape Hatteras today (Mayer, 2002). The impact of the ocean oxic state on hydrate abundance was gauged in simulations with time-uniform forcing, called *Atlantic*, *Pacific*, *OMZ*, and *Anoxic*.

As with the sea level forcing, the depositional trajectory of POC deposition is not intended to mimic any location in particular, but rather to give an indication of how typical deposition cycles might affect the methane cycle in continental margins in general: the sensitivity of the methane cycle to variability in time. High POC concentrations accumulate in a time of high sea level in the simulation, which becomes a buried feature by the end of the simulation (Fig. 9 left).

2.5.2 Biological degradation

Biological degradation is taken to be a function of temperature (T , °C), sediment age, and dissolved methane concentration.

The first exponential term represents the activation energy for respiration, tripling in rate with a temperature increase of 10°C (Wellsbury et al., 1997). The second represents inhibition of biological activity above a critical temperature of 50°C. The formulation uses a smoothed “Heaviside” function to shut down the respiration reactions above a threshold temperature of 50°C. This function is used several times in the SpongeBOB formulation, defined as

$$H_{\text{smooth}}(x, \Delta x) = \frac{1}{\phi} \left(0.5 \arctan \left(\frac{x}{\Delta x} \right) \right)$$

Passive coastal margin deep sedimentary carbon and methane cycles

D. E. Archer et al.

Title Page

Abstract

Introduction

Conclusions

References

Tables

Figures

⏪

⏩

◀

▶

Back

Close

Full Screen / Esc

Printer-friendly Version

Interactive Discussion



The function provides a smooth transition between the on and off states (1 and 0), rather than the discontinuous step function of the true Heaviside function. Raising the function to a power, as done here, tightens the transition, here intended to mimic a fairly strong shutdown of respiration rates when it gets too hot.

The age-dependence mimics the astonishingly wide correlation between carbon age and reactivity observed in nature (Hedges and Keil, 1995). The effect of the “metabolite inhibition” effect as proposed by Wallmann et al. (2006) is represented in the last term in the formulation. Wallmann included dissolved inorganic carbon concentration in addition to methane, but DIC concentrations are too high in the model, perhaps too high (see below), so we took the simplifying liberty of excluding DIC inhibition of methanogenesis.

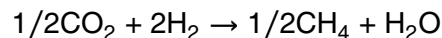
Respiration is concentrated in the top 2 km of the sediment column, limited by temperature (Fig. 10). It is also generally focused offshore of the shelf break, except during periods of very high sea level, during which POC can accumulate in the shelf sediments. When sea level falls, the biologically available POC in the shelf sediment burns out, leaving most of the biological activity in slope sediments, and in particular in the sediment depocenter just off the shelf break. Model sensitivity to the respiration formulation was gauged by varying the “labile fraction” of the POC (cases *Bio 10 %*, *Base* (which is 50 %), and *Bio 100 %*).

2.5.3 Biological methanogenesis

The respiring carbon is assumed to produce DIC and molecular hydrogen, a transient reducing agent. If sulfate is present in the pore water, the hydrogen reduces and consumes it; otherwise, it reacts with CO₂ (DIC) to produce methane in reactions



followed by CO₂ reduction



where the variable x denotes the relative concentration of POH/POC in the reacting organic matter.

The maximum efficiency with which the biologically produced CO_2 can be converted to CH_4 is determined by conservation of carbon, hydrogen, and oxygen from the organic matter to methane plus CO_2 , realizing that supplemental oxygen and hydrogen comes from H_2O . This maximum CH_4 production efficiency is

$$R_{\text{CH}_4} = \frac{1}{2} + \frac{1}{8} \cdot \frac{\text{POH}}{\text{POC}}$$

which works out to 62 % if the H/C ratio of the reacting organic matter is 1. However, carbon isotopic systematics and data, described below, will restrict the efficiency of CH_4 production somewhat, as if about 20 % of the H_2 reacts with oxidized mineral phases such as Fe_2O_3 rather than with CO_2 to make methane, leaving an overall methane production efficiency of about 50 %.

2.5.4 Petroleum and DOC

The model produces petroleum based on chemical and thermal conditions. Petroleum formation in the real world is limited by the H/C ratio of the organic matter, proceeding if the H/C is greater than 1, and continuing until the ratio approaches 1. The temperature dependence of the rate constant is governed by an activation energy of 150 kJ mol^{-1} , with a pre-exponential constant of $1 \times 10^{16} \text{ yr}^{-1}$. These parameters confine petroleum generation to a temperature window of 60–150 °C, as inferred from the distribution of oil (Hunt, 1995).

Petroleum genesis temperatures are too warm to allow bacterial consumption, but 10 % of the oil is assumed upwardly mobile at a rate of 1 m per thousand years. If it reaches cool enough conditions it is consumed by bacterial respiration, following the temperature and solute concentration dependence (but not the POC age dependence) of bacterial POC degradation kinetics above. The rate of methane production by this

BGD

9, 2921–2966, 2012

Passive coastal margin deep sedimentary carbon and methane cycles

D. E. Archer et al.

Title Page

Abstract

Introduction

Conclusions

References

Tables

Figures

⏪

⏩

◀

▶

Back

Close

Full Screen / Esc

Printer-friendly Version

Interactive Discussion

process of “secondary respiration” is shown in Fig. 10b to be deeper than POC respiration, which is more confined to the upper sediment column. The model also assumes “sloppy feeding”, in which 10 % of biological POC consumption goes to dissolved organic carbon (DOC). Simulations to gauge the importance of these processes are called *No Petro* and *No DOC*.

2.5.5 Thermal methanogenesis

Methanogenesis from thermal degradation of organic carbon proceeds according to an Arrhenius equation with an activation energy of 230 kJ mol^{-1} and a pre-exponential rate constant of $4 \times 10^{21} \text{ yr}^{-1}$, which produces a lifetime of a million years at about 160°C . In contrast to the biological rate of methane production, the rate constant for thermal methane generation is very well constrained and consistent in field data, driven by the hunt for petroleum (Hunt, 1995).

The rate of methane production is taken to be this rate constant multiplied by the concentration of particulate organic hydrogen, POH. The POC inventory decreases by 1/4 of the decrease in POH. The distribution of H/C ratio in the sediment column (Fig. 9 right) is primarily driven by the effects of changing ocean chemistry (anoxia) and thermogenic degradation. The H/C ratio approaches zero as the carbon matures, and the decrease in H directly limits the production of methane in the model.

2.5.6 Methane bubbles and hydrate

The dissolved methane concentration is compared with the solubility of dissolved methane, relative to the two possible other phases of gas bubbles or hydrate, in Fig. 11. Disequilibria in the three-phase methane system is restored toward equilibrium by conversion to bubbles or hydrate with a numerically-friendly time constant of 1000 yr. Hydrate or bubbles both release or take up methane from the dissolved phase. When the precise depth of the stability boundary, determined by depth interpolation, falls within a grid cell, the non-gaseous CH_4 is allocated into bubbles and hydrate in proportion to

BGD

9, 2921–2966, 2012

Passive coastal margin deep sedimentary carbon and methane cycles

D. E. Archer et al.

Title Page

Abstract

Introduction

Conclusions

References

Tables

Figures

⏪

⏩

◀

▶

Back

Close

Full Screen / Esc

Printer-friendly Version

Interactive Discussion

the volumes of the two zones, and the concentrations of the phases, for purposes of advection etc., are calculated using the partial grid cell volumes. This prevents a numerical artifact that otherwise appears as the depth of the stability boundary crosses through the numerical grid of the model.

5 A difficult issue to address within SpongeBOB is the mobility and fate of methane gas in the sediment column. The Davie and Buffett (2001) one-dimensional methane hydrate model covers a few hundred meters below the stability zone boundary and assumes that the bubbles are immobile. In the deeper domain of SpongeBOB, if bubbles are not allowed to migrate, gas completely fills some parts of the sediment column
10 pore space (Fig. 12c), so it is clear that gas must be allowed to escape the sediment column in the model. The view from petroleum geology is that, on geologic time scales, sediment columns are permeable to gas, except under permafrost soils and evaporites, which overlay the largest gas accumulations in the world in Siberia and the Middle East, respectively. Other parts of the world, for example the North Sea, are vastly enriched
15 in oil relative to the expected amount of gas were it retained (Hunt, 1995).

Viewed from the perspective of an isolated bubble trapped in a pore space, it is not clear how to get that bubble to move (Jain and Juanes, 2009). The difference in hydrostatic pressure between the top and bottom of a long, interconnected bubble network can be used to drive gas migration. Laboratory experiments find a critical gas saturation of about 10 % where this mechanism begins to kick in (Leas et al., 1950),
20 and values of 1–2 % are often assumed in models for natural gas in wells (Reagan and Moridis, 2007). SpongeBOB, without bubble transport, exceeds these values. But this is an incomplete explanation of bubble mobility in the deep sediment column because it would take an extremely tall bubble to break through the load of a few kilometers of
25 sediment.

We have adopted a parameterization of bubble migration that depends on the bubble fraction in pores

$$\text{CH}_4 \text{ loss} = H_{\text{smooth}}(F_b - 10\%, 5\%)^3$$

Passive coastal margin deep sedimentary carbon and methane cycles

D. E. Archer et al.

Title Page

Abstract

Introduction

Conclusions

References

Tables

Figures



Back

Close

Full Screen / Esc

Printer-friendly Version

Interactive Discussion



where again the H_{smooth} is a smoothed version of a Heaviside function. The bubbles escape as their concentration approaches or exceeds a critical pore volume fraction of 10%. In practical terms, the bubbles in SpongeBOB only fill at most 1–4% of the pore space, because the loss rate, however slow, is able to keep up with production, even when the saturation value is much less than the parameterized critical value.

Rather than resolving the pressures, permeabilities, and flow rates of the bubble phase, for reasons of simplicity, stability, and ease of manipulation, we parameterize the fate of the moving methane gas as an instantaneous redistribution of the moving methane back to the dissolved phase, following a negative exponential function of height in the sediment column. This approach is analogous to the treatment of sinking plankton in the water column of many ocean chemistry models, in which the sinking organic matter is assumed to reach some mean distance before redissolving. The bubbles once in motion rise instantaneously through the sediment until they encounter pore water that is undersaturated with respect to dissolved methane. Once they reach undersaturated conditions the upward flow is attenuated with height into the zone as

$$\text{CH}_4 \text{ flux}(z) = \text{CH}_4 \text{ flux}(0) \cdot e^{-z/z_{\text{scale}}}$$

where the value of the scale height parameter z_{scale} is taken to be 500 m in the high-resolution run, but varied to 100 and 2000 m in two of the sensitivity runs (called *Bubb_100 m* and *Bubb_2 k*).

The distribution of bubbles resulting from these assumptions is shown in Fig. 12. A standing crop of bubbles is sustained by respiration in the upper sediment column, and there is a chimney of bubbles carrying methane from the thermogenic zone up toward the sediment surface. Thermogenic methane in the model systematically evades the hydrate stability zone, because the sediment column is only deep enough to reach high enough temperatures when the top sediment column has nearly reached the sea surface, so that there is in general no hydrate stability zone over thermal methane production in the model (Fig. 12).

Passive coastal margin deep sedimentary carbon and methane cycles

D. E. Archer et al.

Title Page

Abstract

Introduction

Conclusions

References

Tables

Figures

⏪

⏩

◀

▶

Back

Close

Full Screen / Esc

Printer-friendly Version

Interactive Discussion



2.5.7 DIC and subsurface weathering

Measurements of the concentration of dissolved inorganic carbon (DIC) reach ten times higher than the ocean value within the top few hundred meters (what we find to be the respiration zone), and then decrease to half that by the deepest samples measured, about 500 mbsf (Sivan, 2007). The decrease can be explained as a chemical weathering reaction such as



Throughout the upper sediment column, the equilibrium concentration of dissolved CO_2 is much lower than the measured concentrations.

We treated this chemistry as a first-order uptake in DIC. This neglects the impact of the alkalinity or pH of the solution on the CO_2 concentration, but the constancy of porewater alkalinity/DIC ratios (Sivan, 2007) and pH make this seem a reasonable assumption. The kinetics are taken to be a function of temperature as

$$k_{\text{urey}} = 10^{-8+T(C)/0.062}$$

which specifies a reaction timescale of about 10^8 yr at 15°C , so that essentially nothing happens in surface sediments, to a time constant of 1000 yr at 100°C . The effect of the parameterization is to deplete the DIC concentration in the deeper sediment column (Fig. 13, top) relative to the case without the CO_2 drawdown (Fig. 13, bottom). The model DIC concentrations are higher than measured by Sivan et al. (2007), and the penetration deeper, so if anything the model values are underestimates of the rates of CO_2 consumption by the weathering reaction.

The concentration of dissolved inorganic carbon plays several roles in the sedimentary methane cycle. High concentrations of DIC seem to restrict biogenic methane production (Wallmann et al., 2006) although we did not include that here because we couldn't allow the methane cycle to be a slave to a rather out-of-control DIC. The concentration of DIC affects the methane isotope systematics, although as it turns out,

Passive coastal margin deep sedimentary carbon and methane cycles

D. E. Archer et al.

Title Page

Abstract

Introduction

Conclusions

References

Tables

Figures



Back

Close

Full Screen / Esc

Printer-friendly Version

Interactive Discussion



since uptake of by this reaction CO_2 does not fractionate carbon isotopes, the value that emerges in the sediment column does not appear to be a strong function of weathering CO_2 uptake.

2.5.8 Carbon isotopes

5 The model tracks parallel tracers representing the stable carbon isotopes in DIC and CH_4 . The isotopic boundary conditions are that the DIC in the ocean is assumed to be 0‰, and organic matter is assumed -25% . Organic matter is respired to DIC without fractionation. CO_2 reduction carries a fractionation of -90% at 0°C , dropping to about -55% at 50°C (Whiticar and Faber, 1986). Thermogenic methane is assumed to have
10 the isotopic composition of organic matter.

The isotopic composition of DIC in the sediment column (Fig. 14) is lightened by degradation of organic matter, but then pulled heavier by extraction of isotopically light CH_4 . As a result, the isotopic composition of DIC in porewater samples (Sivan et al., 2007) starts near 0‰ at the sediment surface, then trends light in the near subsurface
15 due to respiration in the non-methanogenesis zone, then gets heavier, reaching $+10\%$, at a depth of 500 m (Fig. 14). These authors interpreted the maximum $\delta^{13}\text{C}$ of the DIC as an indicator of the rate of methanogenesis, but it turns out to be more sensitive in the model to the relative partitioning of respired carbon between DIC and methane. If the respired carbon has an isotopic composition of -25% , and the fractionation between CH_4 and DIC at some temperature were 60% , for example, then a balance of
20 about 50% methane versus DIC would tend to produce DIC at an isotopic composition of $+10\%$. In time, this source composition dominates the pore water value. Model experiments did not show a sensitivity of $\delta^{13}\text{C}$ in DIC to the overall methaneogenesis rates, but it does respond to the relative CH_4 production efficiency. The best-fit seems
25 to require some loss of H_2 in the pathway, as if by reduction of mineral phases.

BGD

9, 2921–2966, 2012

Passive coastal margin deep sedimentary carbon and methane cycles

D. E. Archer et al.

Title Page

Abstract

Introduction

Conclusions

References

Tables

Figures

⏪

⏩

◀

▶

Back

Close

Full Screen / Esc

Printer-friendly Version

Interactive Discussion

2.5.9 Iodine 129

Iodine 129 has been used as a tracer for the age of the degrading organic matter in a sediment column (Fehn et al., 2000). Iodine is incorporated into biological material, and it is released to the pore water as the carbon degrades biologically. Both stable and unstable iodine advect with the pore fluid and are subject to diffusion along with the rest of the dissolved tracers. Iodine 129 has a 22.8 million year e-folding lifetime and it is produced by cosmic ray spallation in the atmosphere. Iodine released by older organic carbon will have less Iodine-129 because of radioactive decay. Fehn et al. (2000) measured I^{129} ages 55 million years old in pore waters of solid sediment that was 1.8 to 6 million years old, a difference of about 50 million years. Fehn et al. (2000) interpreted this as indicative of 50 million year old carbon degrading.

Iodine 129 seems like a very rich tracer in the SpongeBOB model, indicative of the history of the accumulation of the sediment column and the expulsion of fluid from it. The iodine ages of the pore waters are higher than those of the solids, in near-surface sediments, while in the deepest sediment column the pore fluid iodine is much younger than the solid phase (Fig. 15a). When permeable vertical conduits are available, the ages within the conduit are older than in the surrounding low-flow columns (Fig. 15b), but the conduits do not change the fundamental pattern. These patterns are caused fundamentally by the compaction-driven upward flow of the pore water. When fluid flow is prevented in the model, the iodine ages collapse to the sediment ages (Fig. 15c).

The iodine ages in the depth range of Blake Ridge in SpongeBOB never get as old as Fehn et al. (2000) measured at Blake Ridge. The values in the conduits reach 20 million years old, while Fehn measured 50 million years. It could be that Blake Ridge is affected by focused subsurface flow such as crudely approximated by the model, or it could be that a recent decrease in sedimentation rate has affected Blake Ridge.

BGD

9, 2921–2966, 2012

Passive coastal margin deep sedimentary carbon and methane cycles

D. E. Archer et al.

Title Page

Abstract

Introduction

Conclusions

References

Tables

Figures

⏪

⏩

◀

▶

Back

Close

Full Screen / Esc

Printer-friendly Version

Interactive Discussion

3 Results

3.1 Model Sensitivity Runs

In addition to the “Base HR” and “No Conduits HR” cases, a series of sensitivity simulations were done, at lower spatial resolution of only 10 grid points horizontally instead of 40. The setup, intent, and summary of the conclusions from the sensitivity runs are described in Tables 1 and 2. One suite of simulations was forced by time-invariant forcing, comprising sea level, ocean “oxic” state (POC deposition patterns), and temperature, with variations as described in Table 1. These allow a clearer diagnosis of the model sensitivity to these variables. Another suite of simulations imposes time-varying forcing shown in Fig. 4, as described in Table 2. The time evolution of sea level, POC inventory, methanogenesis rates, and hydrate inventories are shown in Fig. 16c for the two representative cases, the *Base* case, which including the sea level changes, and case T0, which does not.

3.2 Sensitivity to ocean temperature

The effect of ocean temperature on model hydrate inventory is shown in Fig. 17a. These are from time-invariant suite of runs, with temperature a function of water depth only. The inventory of hydrate decreases roughly linearly with temperature, finally reaching zero hydrate with a warming of 10°C. The active margin simulations (presented in the companion paper) have a similar temperature sensitivity to the passive case. The SpongeBOB model is significantly less sensitive to temperature than the Davie and Buffett (2001) one-dimensional model (Fig. 17a). These are essentially equilibrium calculations, comparable to those of Buffett and Archer (2004).

The difference is probably due to the fundamentally different processes controlling vertical methane fluxes between the two models. The 1-D model relies on the transport of dissolved-phase methane into the stability zone. In a warmer ocean, the stability zone gets thinner, which increases the diffusive loss of dissolved methane in that model

BGD

9, 2921–2966, 2012

Passive coastal margin deep sedimentary carbon and methane cycles

D. E. Archer et al.

Title Page

Abstract

Introduction

Conclusions

References

Tables

Figures

⏪

⏩

◀

▶

Back

Close

Full Screen / Esc

Printer-friendly Version

Interactive Discussion



by requiring the diffusive gradient to be steeper. This had the impact of restricting the formation of hydrate to regions of higher POC content, reducing the ocean's ultimate equilibrium inventory of methane nearly completely with 3°C of warming. Methane trapping in the stability zone, when it is transported by bubbles in SpongeBOB, would also be affected by a change in the stability zone thickness, but the mechanism is different and so it is not surprising that the two models would have different temperature sensitivity.

3.3 Sensitivity to POC

The model sensitivity to POC deposition was gauged using time-invariant forcing, by varying the “ocean oxic state” variable through the spectrum from “*Atlantic*” (low POC concentrations in surface sediments, state = 1) to “*Pacific*” (2), “*OMZ*” (3), and “*Anoxic*” (4). The range in sediment surface POC concentrations is intended to bracket something of the range in the ocean, and Fig. 17b shows the sensitivity to that range. These variations in POC deposition have a much stronger impact on the hydrate inventory than the temperature does. This is consistent with the recent finding of Gu et al. (2011)

The sensitivity of the hydrate inventory can also be seen in the model response to changes in the labile fraction of the sedimenting POC (Fig. 17c). In practice, the respiration zone is thin enough that the POC is not often limited by depletion of the labile POC fraction, so the labile fraction acts like a scaling of the apparent bulk POC degradation rate constant. With the tight correlation between organic carbon age and reaction rate (Middelburg et al., 1997), this range in effective POC degradation rate constants might optimistically be viewed as a range in the uncertainty in the POC degradation rates.

The sensitivity to biologically labile POC in particular shows that biogenic methane production is the important factor in the model. A model sensitivity run with thermogenic methane production disabled (called *No Therm*) corroborates this by the lack of much change in the hydrate inventory. Secondary respiration of migrating petroleum, simulation *No Petro*, produces no hydrate, a strong effect to be sure. However, the absence

Passive coastal margin deep sedimentary carbon and methane cycles

D. E. Archer et al.

Title Page

Abstract

Introduction

Conclusions

References

Tables

Figures

⏪

⏩

◀

▶

Back

Close

Full Screen / Esc

Printer-friendly Version

Interactive Discussion



of hydrate without petroleum migration in the model does not mean that petroleum is the whole story. The hydrate inventory is so responsive to reasonable changes primary POC respiration that were we to neglect secondary petroleum respiration in the model, the primary respiration could be increased enough to tip back over to the point of preserving hydrate.

The time evolution of hydrate between the time-variant and –invariant configurations also demonstrates the primacy of POC forcing over temperature forcing for the model. In the time-variant configuration (*Base*), there is more hydrate in the middle of the simulation when sea level is high and the ocean warm than there at the end of the simulation, supposed to be cold and low-POC like today. The warm temperatures of the hothouse were more than offset by the increase in POC deposition. The hydrate inventory declines in the transition from the hothouse to the icehouse, rather than growing. In contrast, the time-invariant model hydrate inventory (the base case of which is called *T0*) peaks strongly at the end of the simulation, reflecting the larger sediment mass perhaps. The trajectories of hydrate inventory follow those of POC inventory and methanogenesis rates, rather than temperature or sea level (Fig. 16).

All three indications of hydrate inventory sensitivity to biogenic methane production rates indicate that this variable is more important to get right than the temperature.

3.4 Sensitivity to bubble transport

The hydrate inventory in the model depends critically on methane transport by rising bubbles through the sediment column, and redissolution if the bubbles enter an undersaturated condition. This mechanism is novel to SpongeBOB, not shared by the Davie and Buffett (2001) or other 1-D models. If bubble transport is disabled, hydrate disappears from the results (Fig. 16). Figure 17d shows the extreme model sensitivity to the redissolution height scale, which determines what fraction of the methane will be recaptured by redissolution rather than escape directly to the sea floor. When a scale height of 2 km is imposed, hydrate again disappears from the simulation. Shortening the height scale from 500 m to 100 m increases the hydrate inventory by a factor of

BGD

9, 2921–2966, 2012

Passive coastal margin deep sedimentary carbon and methane cycles

D. E. Archer et al.

Title Page

Abstract

Introduction

Conclusions

References

Tables

Figures



Back

Close

Full Screen / Esc

Printer-friendly Version

Interactive Discussion



nearly 8. Clearly this is a parameter to which the model is very sensitive, and which requires further work to capture the complexity of the real world in a numerical model.

3.5 Pore fluid flow heterogeneity

Old iodine 129 ages in pore waters at Blake Ridge, relative to the age of the solids, can only be reproduced in the model as resulting from heterogeneity in the pore fluid flow field, as crudely mimicked in the code by the vertical high-permeability chimneys. This conclusion is reinforced by the heterogeneity in penetration depth for dissolved sulfate, SO_4^{2-} (Borowski et al., 1996), which seem to show a bimodal distribution, with some sites where the methane/sulfate boundary is just a few 10's of meters, and others where sulfate reaches hundreds of meters or more. The shallow sites correlate with the presence of methane hydrate, just like in the model where the hydrate is found. The importance of the chimneys justifies the imposition of an upward flow in the Davie and Buffett one-dimensional model (2001), which was interpreted as representing a zone of upward flow, analogous to the chimneys here.

3.6 Other model (in)sensitivities

Most of the other scenarios had a fairly minor impact on the hydrate inventory. Thermogenic methane is not a significant contributor to the pelagic hydrate methane pool. The permeable chimneys do not determine the solution, nor does sediment erosion and redeposition, or the value of the critical seafloor slope that drives it.

4 Conclusions

Our attempt to capture the carbon and methane cycles of the entire sediment column have led us to make a choice in model formulation which might serve as a hypothesis for the real world. Bubble migration through the sediment column seems crucial to getting SpongeBOB to work, and appears to be important in the real sediment column,

Passive coastal margin deep sedimentary carbon and methane cycles

D. E. Archer et al.

Title Page

Abstract

Introduction

Conclusions

References

Tables

Figures



Back

Close

Full Screen / Esc

Printer-friendly Version

Interactive Discussion



but it needs more attention both in the field and in the model. It turns out that the hydrate inventory in the simulations depended very strongly on the scale height for methane redissolution if a bubble enters an undersaturated zone.

Heterogeneity in the vertical flow field, simulated very crudely in SpongeBOB as vertical chimneys of increased permeability, increases the global inventory of hydrate, determines where the hydrate will be found, and it will affect chemical tracers such as iodine 129, and the depth of SO_4^{2-} penetration in the sediment column, which corroborate the conclusion that the hydrate distribution is steered by upward flow.

The model is also very sensitive to organic carbon rain to the sea floor; more sensitive to a reasonable range of sedimentary organic carbon concentrations than to the range of temperatures going back through geologic time.

Supplementary material related to this article is available online at:

<http://www.biogeosciences-discuss.net/9/2921/2012/>

[bgd-9-2921-2012-supplement.zip](#).

Acknowledgements. This project was funded by DOE NETL project DE-NT0006558. Plots were done using Ferret, a product of NOAA's Pacific Marine Environmental Laboratory (<http://ferret.pmel.noaa.gov/Ferret/>).

References

Archer, D. E., Morford, J. L., and Emerson, S. R.: A model of suboxic sedimentary diagenesis suitable for automatic tuning and gridded global domains, *Global Biogeochem. Cy.*, 16, 1017, doi:10.1029/2000GB001288, 2002.

Athy, L. F.: Density, porosity and compaction of sedimentary rocks, *AAPG Bull.*, 14, 1–24, 1930.

Borowski, W. S.: A review of methane and gas hydrates in the dynamic, stratified system of the Blake Ridge region, offshore southeastern North America, *Chem. Geol.*, 205, 311–346, 2004.

Borowski, W. S., Paull, C. K., and Ussler, W.: Marine pore-water sulfate profiles indicate in situ methane flux from underlying gas hydrate, *Geology*, 24, 655–658, 1996.

BGD

9, 2921–2966, 2012

Passive coastal margin deep sedimentary carbon and methane cycles

D. E. Archer et al.

Title Page

Abstract

Introduction

Conclusions

References

Tables

Figures

◀

▶

◀

▶

Back

Close

Full Screen / Esc

Printer-friendly Version

Interactive Discussion



Passive coastal margin deep sedimentary carbon and methane cycles

D. E. Archer et al.

Title Page

Abstract

Introduction

Conclusions

References

Tables

Figures

⏪

⏩

◀

▶

Back

Close

Full Screen / Esc

Printer-friendly Version

Interactive Discussion



- Buffett, B., and Archer D. E.: Global inventory of methane clathrate: Sensitivity to changes in environmental conditions, *Earth Planet. Sci. Lett.*, 227, 185–199, 2004.
- Daigle, H. and Dugan, B.: Permeability anisotropy and fabric development: A mechanistic explanation, *Water Resour. Res.*, 47, W12517, doi:10.1029/2011WR011110, 2011.
- 5 Davie, M. K. and Buffett, B. A.: A numerical model for the formation of gas hydrate below the seafloor, *J. Geophysical Res.*, 106, 497–514, 2001.
- Davie, M. K. and Buffett, B. A.: Sources of methane for marine gas hydrate: inferences from a comparison of observations and numerical models, *Earth Planet. Sci. Lett.*, 206, 51–63, 2003a.
- 10 Davie, M. K. and Buffett, B. A.: A steady state model for marine hydrate formation: Constraints on methane supply from pore water sulfate profiles, *J. Geophysical Res.*, B10, 2495, doi:10.1029/2002JB002300, 2003b.
- Fehn, U., Snyder, G., and Egeberg, P. K.: Dating of pore waters with I-129: Relevance for the origin of marine gas hydrates, *Science*, 289, 2332–2335, 2000.
- 15 Flemings, B. P., Liu, X., and Winters, W. J.: Critical pressure and multiphase flow in Blake Ridge gas hydrates, *Geology*, 31, 1057–1060, 2003.
- Flemings, P. B., Stump, B. B., Finkbeiner, T., and Zoback, M.: Flow focusing in overpressured sandstones: Theory, observations, and applications, *Am. J. Sci.*, 302, 827–855, 2002.
- Gu, G., Dickens, G. R., Bhatnagar, G., Colwell, F. S., Hirasaki, G. J., and Chapman, A. G.:
 20 Abundant Early Palaeogene marine gas hydrates despite warm deep-ocean temperatures, *Nature Geosci.*, 4, 848–851, 2011.
- Haq, B. U., Hardenbol, P. R., and Vail, P. R.: Chronology of fluctuation sea levels since the Triassic, *Science*, 235, 1156–1167, 1987.
- Hedges, J. I., and Keil, R. G.: Sedimentary organic matter preservation an assessment and
 25 speculative synthesis, *Mar. Chem.*, 49, 81–115, 1995.
- Hunt, J. M.: *Petroleum Geochemistry and Geology*, Freeman, New York, USA, 743 pp., 1995.
- Jain, A. K. and Juanes, R.: Preferential Mode of gas invasion in sediments: Grain-scale mechanistic model of coupled multiphase fluid flow and sediment mechanics, *J. Geophys. Res.-Sol. Earth*, 114, B08101, doi:10.1029/2008JB006002, 2009.
- 30 Kennett, J. P., *Marine Geology*, Prentice-Hall, Englewood Cliffs, NJ, USA, 813 pp., 1982.
- Leas, W. J., Jenks, L. H., and Russell, C. D.: Relative permeability got gas, *Trans. AIME*, 189, 65–72, 1950.

Passive coastal margin deep sedimentary carbon and methane cycles

D. E. Archer et al.

Title Page

Abstract

Introduction

Conclusions

References

Tables

Figures

⏪

⏩

◀

▶

Back

Close

Full Screen / Esc

Printer-friendly Version

Interactive Discussion



- Mayer, L.: Mineral associations and nutritional quality of organic matter in shelf, Deep-Sea Res. Part II – Top. Stud. Oceanogr., 49, 4587–4597, 2002.
- Meiburg, E and B. Kneller, Turbidity currents and their deposits, Ann. Rev. Fluid Mech., 42, 135–156, 2010.
- 5 Middelburg, J. J., Soetaert, K., and Herman, P. M. J.: Empirical relations for use in global diagenetic models, Deep-Sea Res. I, 44, 327–344, 1997.
- Parson, B., and Sclater, J. B.: An analysis of the variations in ocean floor bathymetry and heat flow with age, J. Geophys. Res., 82, 803–827, 1977.
- Pirmez, C., Pratson, L. F., and Steckler, M. S.: Clinoform development by advection-diffusion of
 10 suspended sediment: Modeling and comparison to natural systems, J. Geophys. Res.-Sol. Earth, 103, 24141–24157, 1998.
- Reagan, M. T. and Moridis, G. J.: Oceanic gas hydrate instability and dissociation under climate change scenarios, Geophys. Res. Lett., 34, L22709, doi:10.1029/2007GL031671, 2007.
- Sivan, O., Schrag, D. P., and Murray, R. W.: Rates of methanogenesis and methanotrophy in
 15 deep-sea sediments, Geobiology, 5, 141–151, 2007.
- Strobel, J., Cannon, R., Christopher, G. St., Kendall, C. St., Biswas, G., and Bezdek, J.: Interactive (SEDBAK) simulation of clastic and carbonate sediments in shelf to basin settings, Comput. Geosci., 15, 1279–1290, doi:10.1016/0098-3004(89)90092-7, 2003.
- Syvitski, J. P. M. and Hutton, E. W. H.: 2D SEDFLUX 1.0C: an advanced process-response
 20 numerical model for the fill of marine sedimentary basins, Comput. Geosci., 27, 731–753, 2001.
- Wallmann, K., Aloisi, G., Haeckel, M., Obzhirov, A., Pavlova, G., and Tishchenko, P.: Kinetics of organic matter degradation, microbial methane generation and gas hydrate formation in anoxic marine sediments, Geochim. Cosmochim. Acta, 70, 3905–3927, 2006.
- 25 Wellsbury, P., Goodman, K., Barth, T., Cragg, B. A., Barnes, S. P., and Parkes, J.: Deep marine biosphere fuelled by increasing organic matter availability during burial and heating, Nature, 388, 573–576, 1997.
- Whiticar, M. J. and Faber, E.: Methane Oxidation in Sediment and Water Column Environments – Isotope Evidence, Org. Geochem., 10, 759–768, 1986.

Passive coastal margin deep sedimentary carbon and methane cycles

D. E. Archer et al.

Table 1. Model scenarios with uniform sea level and POC deposition state (ocean oxic state = 3).

T0	No temperature offset	Higher hydrate than the Base case because of higher POC rain in the last bits of the simulation
<i>T2, T4</i> etc.	2, 4, 6, 8, and 10°C temperature increases	Weaker temperature sensitivity than the 1-D models (Fig. 17)
Atl, Pac, Anoxic	“Atlantic” (ocean state 1) “Pacific” (state 2), and “Anoxic” (state 4) POC rain forcings, shown in Fig. 4. Default is state 3 in the T^* runs.	Stronger POC dependence for this range of conditions than T dependence

Title Page

Abstract

Introduction

Conclusions

References

Tables

Figures

⏪

⏩

◀

▶

Back

Close

Full Screen / Esc

Printer-friendly Version

Interactive Discussion



Passive coastal margin deep sedimentary carbon and methane cycles

D. E. Archer et al.

Title Page

Abstract

Introduction

Conclusions

References

Tables

Figures

⏪

⏩

◀

▶

Back

Close

Full Screen / Esc

Printer-friendly Version

Interactive Discussion

Table 2. Simulations with a time-varying sea level and ocean oxic state (POC deposition).

Simulation name	Characteristics	Salient results
Base	Base case	
Lores Base	Lower resolution version of the full base case for comparison with sensitivity runs	Nearly 50 % less hydrate than the higher resolution case
No Conduits	Vertical permeable chimneys eliminated	Similar hydrate inventory to Lores Base
Labile 10 %, Labile 100 %	Changed the biologically-available POC fraction from 50 % in base to 10 % and 100 %	Nearly linear dependence of hydrate inventory on rate constant.
No Bubb Mig	Bubble migration disabled	Eliminates hydrate
Bubb Mig 100 m, Bubb Mig 2 km	Redissolution height scale for rising bubbles from 500 m in base to 100 m and 2 km	Strong impact on hydrate inventory
Lo Slope	The maximum sea floor slope is taken to be 3 % instead of 6 % in base	No strong hydrate inventory impact
No Slides	Landslides disabled	No strong hydrate inventory impact
No Thermogen	Thermal methanogenesis disabled	No strong hydrate inventory impact
No Petroleum	Petrogenesis disabled	Eliminates hydrate
No DOC	DOC production and respiration disabled	No strong hydrate inventory impact

Passive coastal margin deep sedimentary carbon and methane cycles

D. E. Archer et al.

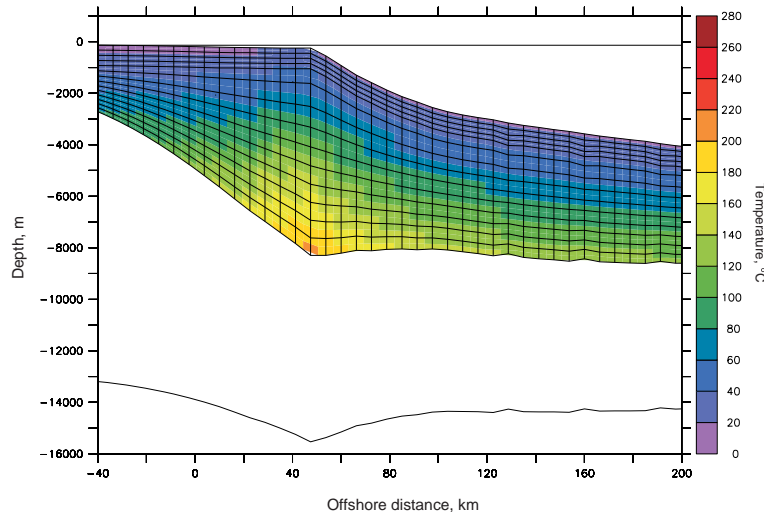


Fig. 1. SpongeBOB in isostatic equilibrium. Colors are temperatures on the computational grid of the model, traced horizontally by the black lines. The thickness of the underlying crust grades from thin ocean crust on the right side of the domain into a thicker (and less dense) continental crust on the left. The transition between ocean and continental crust is smoothed over a spatial scale of 25 km. Local isostasy applies, on a time scale of 10 000 yr and with spatial smoothing over 20 km. An animation of the simulation can be viewed at http://geosci.uchicago.edu/~archer/spongebob_passive/fig1.atlantic.movie.gif and in the Supplement.

Title Page

Abstract

Introduction

Conclusions

References

Tables

Figures

◀

▶

◀

▶

Back

Close

Full Screen / Esc

Printer-friendly Version

Interactive Discussion

Passive coastal margin deep sedimentary carbon and methane cycles

D. E. Archer et al.

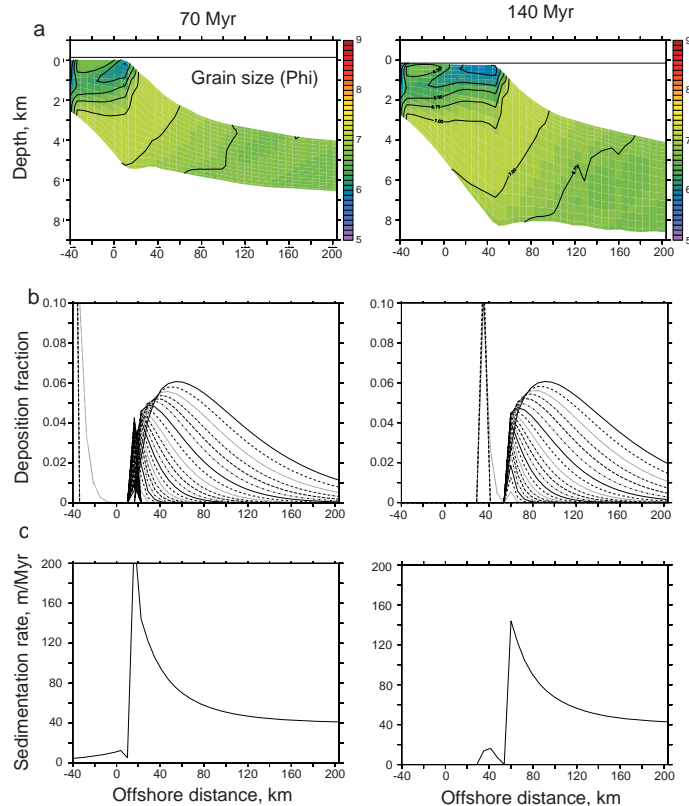


Fig. 2. Sediment transport model results. **(a)** Mean grain size ($\phi = \log_{10}(\text{mm})$) in the sediment column half-way through (left) and at the end of the simulation (right). **(b)** Snapshots of the sedimentation rate of particles of various sizes. **(c)** Snapshots of the total sedimentation rate, with a depocenter just off the shelf break. An animation of this figure can be viewed at http://geosci.uchicago.edu/~archer/spongebob_passive/fig2.atlantic.movie.gif and in the Supplement.

Passive coastal margin deep sedimentary carbon and methane cycles

D. E. Archer et al.

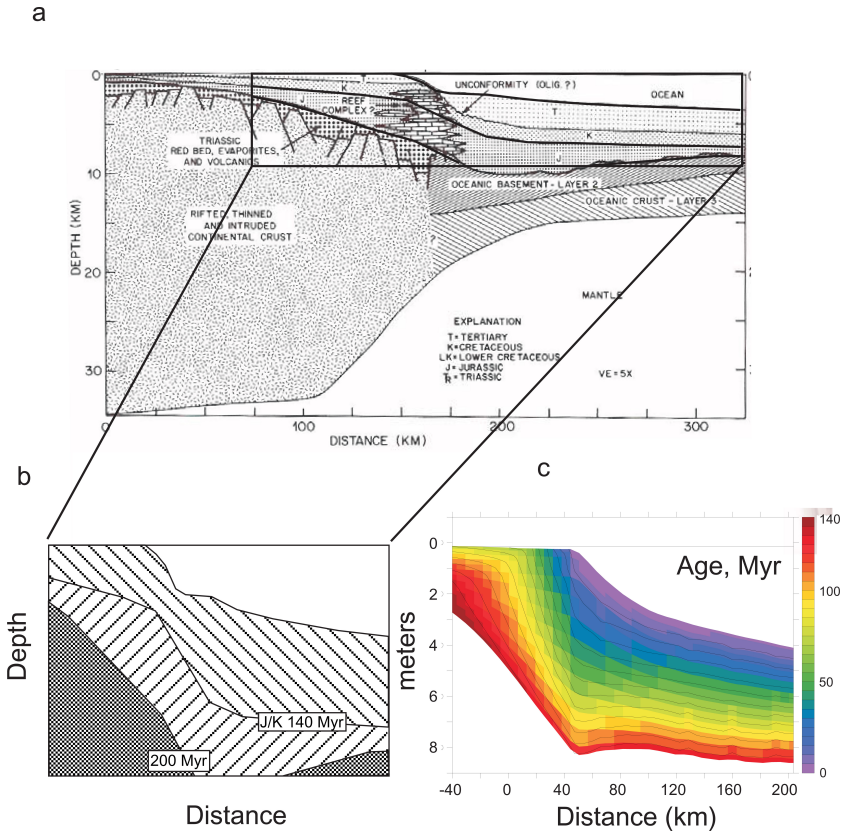


Fig. 3. (a) Sediment column constructed from a seismic section off Cape Cod, from Kennett (1982), with cutout (b) resized for comparison with model results (c).

Title Page

Abstract Introduction

Conclusions References

Tables Figures

◀ ▶

◀ ▶

Back Close

Full Screen / Esc

Printer-friendly Version

Interactive Discussion

Passive coastal margin deep sedimentary carbon and methane cycles

D. E. Archer et al.

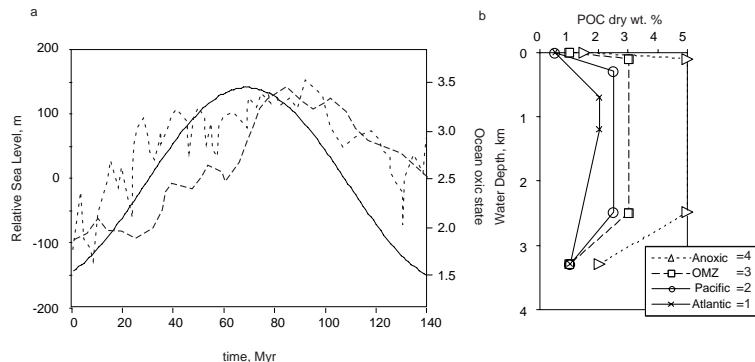


Fig. 4. (a) Sea level time variation with time imposed on the simulation, and corollary changes in the “ocean state”, which drive POC deposition concentration patterns as in (b), where Atlantic and Pacific represent conditions typical of the East or Northwest coasts of United States, “OMZ” is stronger oxygen minimum conditions typical of the Eastern equatorial Pacific, and Anoxic refers to anoxic conditions. Concentrations of POC in ocean sediments vary through this range and beyond; the intent here is to allow for variations that span something like the observed range.

Discussion Paper | Discussion Paper | Discussion Paper | Discussion Paper | Discussion Paper

Title Page

Abstract

Introduction

Conclusions

References

Tables

Figures

◀

▶

◀

▶

Back

Close

Full Screen / Esc

Printer-friendly Version

Interactive Discussion



Passive coastal margin deep sedimentary carbon and methane cycles

D. E. Archer et al.

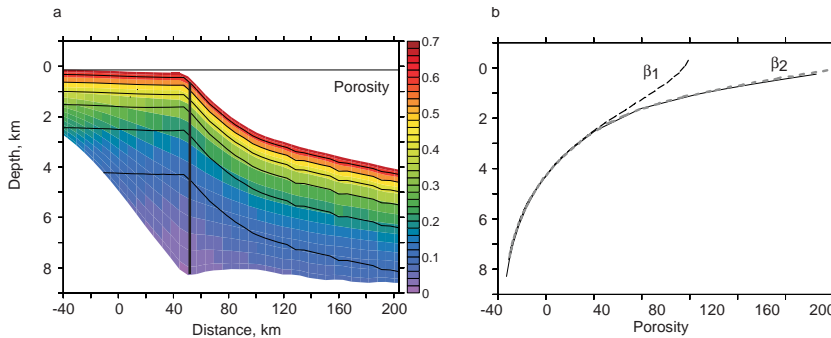


Fig. 5. Porosity at the end of the simulation, section **(A)** and profile **(b)** taken on the heavy solid line in **(a)**: (solid line) full model solution, (long dashes) “drained” porosity contribution from β_1 , (short grey dashes) sum of drained porosity contribution from $\beta_1 + \beta_2$.

Title Page

Abstract

Introduction

Conclusions

References

Tables

Figures

◀

▶

◀

▶

Back

Close

Full Screen / Esc

Printer-friendly Version

Interactive Discussion

Passive coastal margin deep sedimentary carbon and methane cycles

D. E. Archer et al.

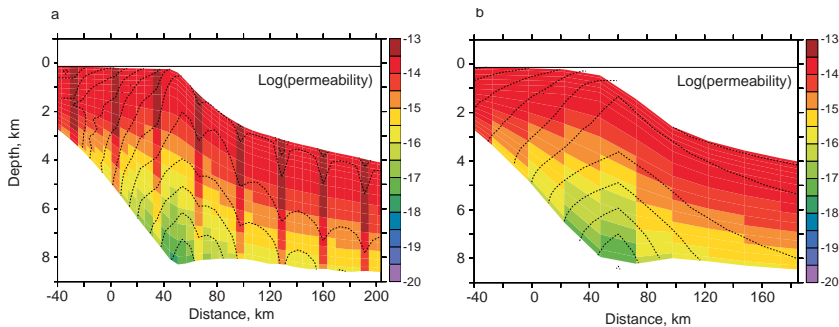


Fig. 6. Log of the permeability from the end of the simulation, **(a)** from the Base case and **(b)** the No Chan case with the vertical permeable chimneys disabled and at lower horizontal resolution.

[Title Page](#)[Abstract](#)[Introduction](#)[Conclusions](#)[References](#)[Tables](#)[Figures](#)[⏪](#)[⏩](#)[◀](#)[▶](#)[Back](#)[Close](#)[Full Screen / Esc](#)[Printer-friendly Version](#)[Interactive Discussion](#)

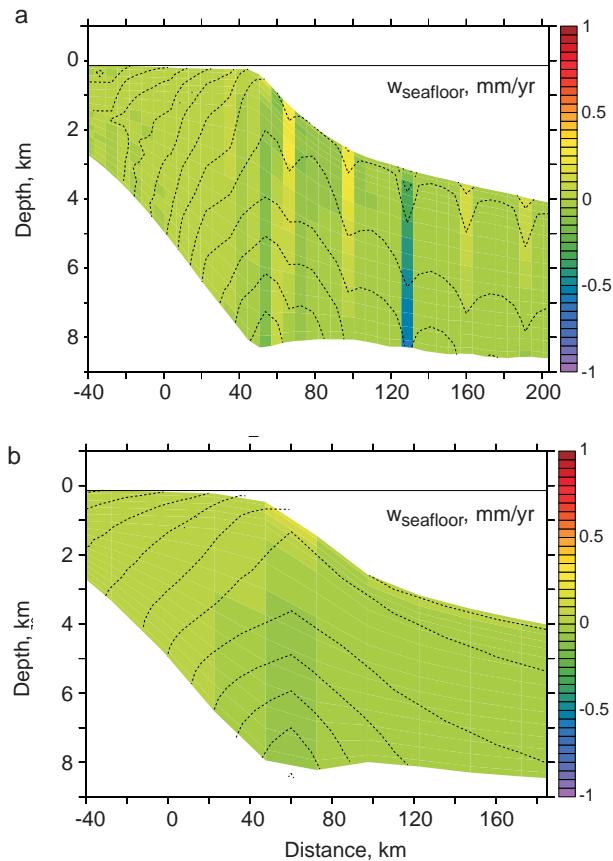


Fig. 7. Vertical velocity relative to the moving sea floor (w_{seafloor}) for the Base **(a)** and No Chimneys **(b)** cases, from the end of the simulation. An animation of the simulation can be viewed at http://geosci.uchicago.edu/~archer/spongebob_passive/w_seafloor.movie.gif and in the Supplement.

Passive coastal margin deep sedimentary carbon and methane cycles

D. E. Archer et al.

Title Page

Abstract Introduction

Conclusions References

Tables Figures

⏪ ⏩

◀ ▶

Back Close

Full Screen / Esc

Printer-friendly Version

Interactive Discussion



Passive coastal margin deep sedimentary carbon and methane cycles

D. E. Archer et al.

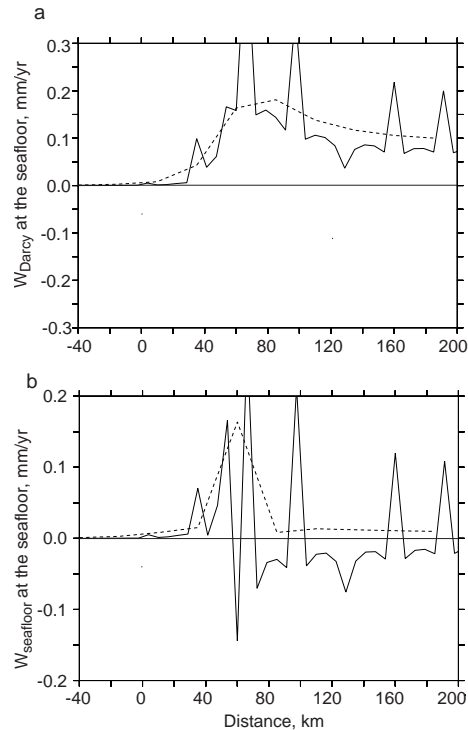


Fig. 8. Rates of vertical flow at the sea floor. Solid lines are the Base scenario, dashed the No Chimney run. **(a)** Darcy flows (w_{Darcy}) are upward, while **(b)** flows relative to the moving seafloor (w_{seafloor}) can be found in both directions. An animation of the simulation can be viewed at http://geosci.uchicago.edu/~archer/spongebob_passive/w_seafloor_sf.movie.gif in the Supplement.

Title Page

Abstract

Introduction

Conclusions

References

Tables

Figures

◀

▶

◀

▶

Back

Close

Full Screen / Esc

Printer-friendly Version

Interactive Discussion

Passive coastal margin deep sedimentary carbon and methane cycles

D. E. Archer et al.

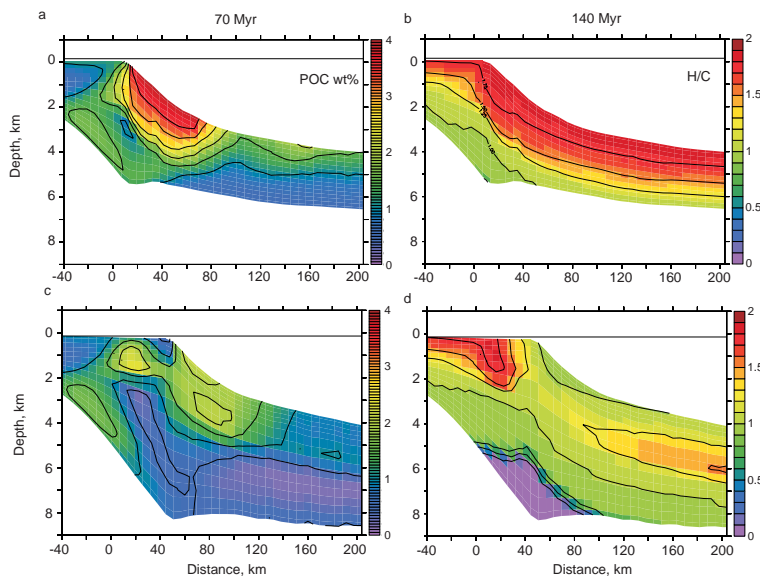


Fig. 9. POC concentrations (dry weight percent) (**a** and **c**) and H/C elemental ratio of organic matter (**b** and **d**). From half-way through (**a** and **b**) the simulation, at a period of high sea level, and (**c** and **d**) at the end of the simulation, when sea level is relatively low, as today. An animation of the simulation can be viewed at http://geosci.uchicago.edu/~archer/spongebob_passive/poc.movie.gif and in the Supplement.

Title Page

Abstract

Introduction

Conclusions

References

Tables

Figures

◀

▶

◀

▶

Back

Close

Full Screen / Esc

Printer-friendly Version

Interactive Discussion

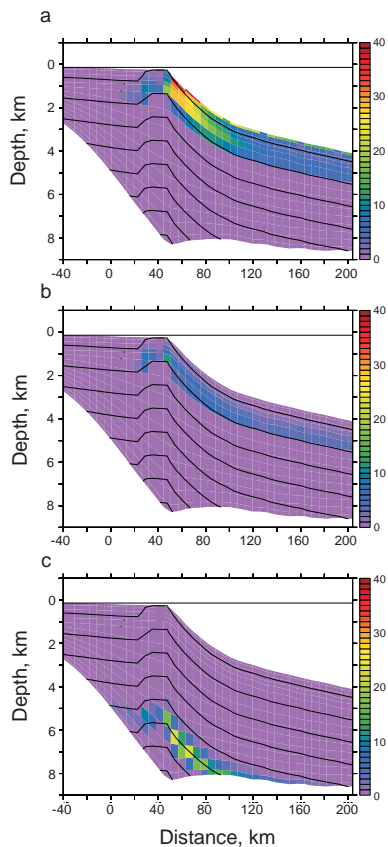


Fig. 10. Methane sources in the sediment column. **(a)** From biological respiration of POC. **(b)** From biological degradation of migrating petroleum. **(c)** From thermal alteration of POC. An animation of the simulation can be viewed at http://geosci.uchicago.edu/~archer/spongebob-passive/ch4_src.movie.gif and in the Supplement.

Passive coastal margin deep sedimentary carbon and methane cycles

D. E. Archer et al.

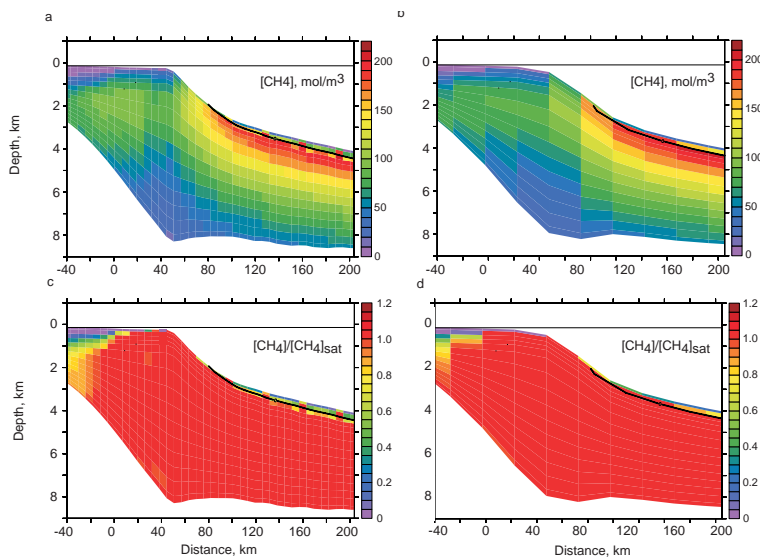


Fig. 11. Concentration of dissolved methane plotted in moles m^{-3} (**a** and **b**), and relative to saturation (**c** and **D**). Base model run (**a** and **c**), and No Chimneys (**b** and **d**). An animation of the simulation can be viewed at http://geosci.uchicago.edu/~archer/spongebob_passive/ch4.movie.gif and in the Supplement.

Title Page

Abstract

Introduction

Conclusions

References

Tables

Figures

◀

▶

◀

▶

Back

Close

Full Screen / Esc

Printer-friendly Version

Interactive Discussion

Passive coastal margin deep sedimentary carbon and methane cycles

D. E. Archer et al.

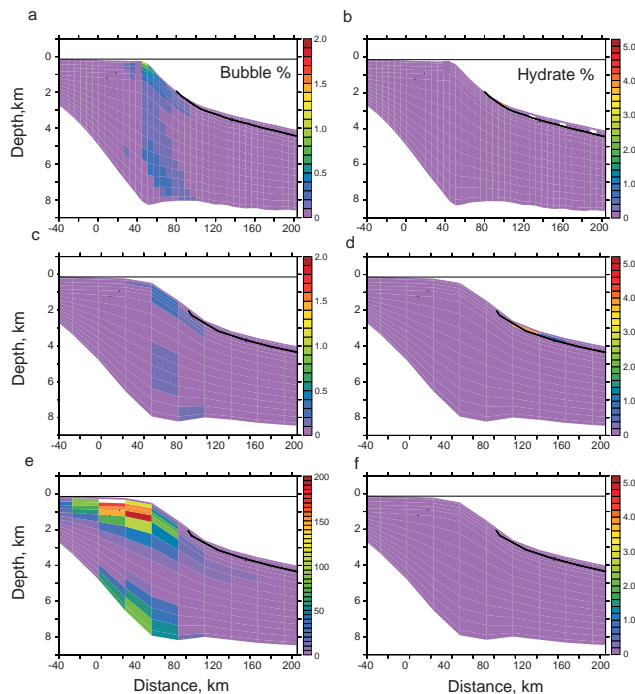


Fig. 12. Bubbles (**a, C, e**) and hydrate (**B, d, f**) (volume percent of pore space). From the Base model (**a** and **b**), the No Chimneys model (**c** and **d**), and with bubble migration disabled (**e** and **f**). An animation of the simulation can be viewed at http://geosci.uchicago.edu/~archer/spongebob_passive/bubbles.movie.gif and in the Supplement.

Title Page

Abstract Introduction

Conclusions References

Tables Figures

⏪ ⏩

◀ ▶

Back Close

Full Screen / Esc

Printer-friendly Version

Interactive Discussion



Passive coastal margin deep sedimentary carbon and methane cycles

D. E. Archer et al.

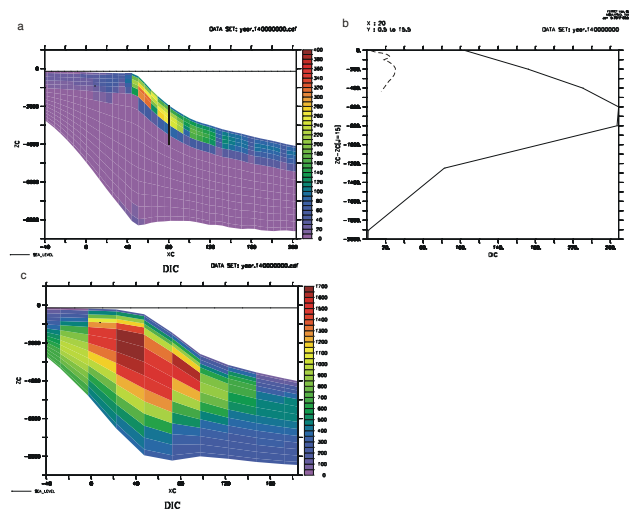


Fig. 13. DIC concentrations, moles m^{-3} . **(a)** Base case section, **(b)** Base case profile compared with data from Sivan et al. (2007), dashed line, and **(c)** with Urey reactions that consume CO_2 disabled (note change in color scale from **a**). An animation of the simulation can be viewed at http://geosci.uchicago.edu/~archer/spongebob_passive/dic.movie.gif and in the Supplement.

Title Page

Abstract

Introduction

Conclusions

References

Tables

Figures

◀

▶

◀

▶

Back

Close

Full Screen / Esc

Printer-friendly Version

Interactive Discussion

Passive coastal margin deep sedimentary carbon and methane cycles

D. E. Archer et al.

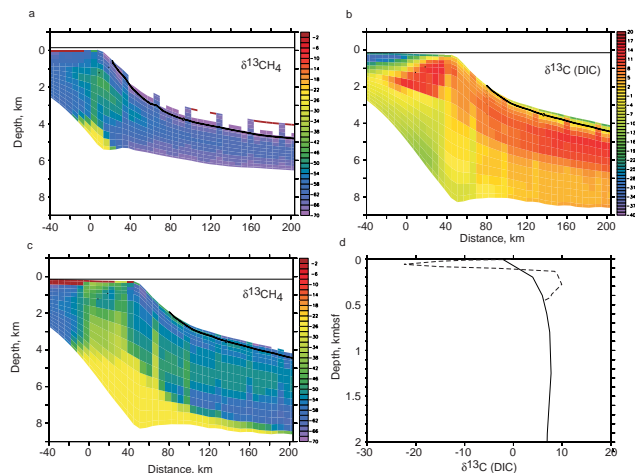


Fig. 14. Carbon isotopic composition of methane from half-way through **(a)**, where little influence of thermogenic methane can be seen, and at the end of the simulation **(c)**, where thermogenic methane can clearly be seen. **(b)** is the $\delta^{13}\text{C}$ of DIC at the end of the simulation, compared with data from Sivan et al. (2007) (dashed line) in profile **(d)**. The model lacks the resolution to capture the isotopically light spike just below the sea floor, but the deep isotopic composition matches well. Animations of this plot can be viewed at http://geosci.uchicago.edu/~archer/spongebob_passive/del13.movie.gif and in the Supplement.

Title Page

Abstract

Introduction

Conclusions

References

Tables

Figures

◀

▶

◀

▶

Back

Close

Full Screen / Esc

Printer-friendly Version

Interactive Discussion

Passive coastal margin deep sedimentary carbon and methane cycles

D. E. Archer et al.

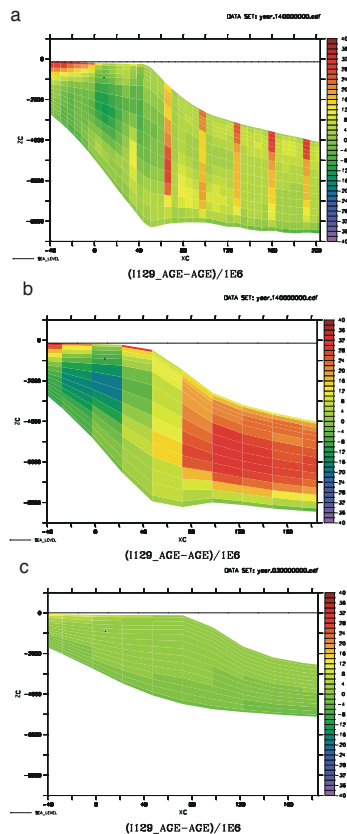


Fig. 15. Iodine-129 porewater age – sediment age, in millions of years. **(a)** With permeable chimneys, **(b)** without permeable chimneys, and **(c)** with pore fluid flow disabled, $t = 30$ myr instead of 140 myr for the other simulations. Animations of this plot can be viewed at http://geosci.uchicago.edu/~archer/spongebob_passive/i129.movie.gif in the Supplement.

Passive coastal margin deep sedimentary carbon and methane cycles

D. E. Archer et al.

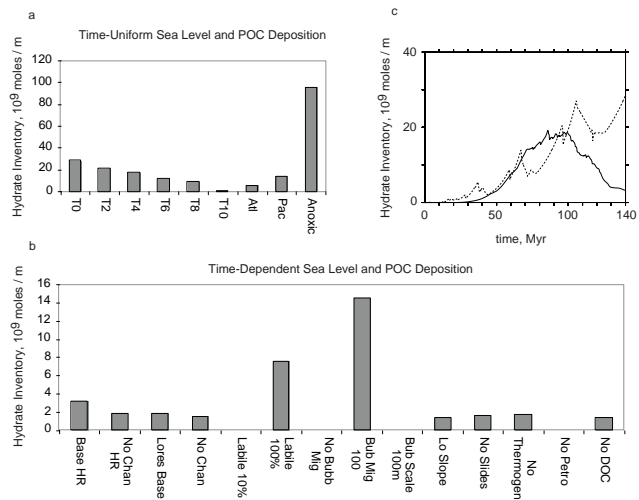


Fig. 16. Results of model sensitivity runs. **(a and b)** Hydrate inventory at the end of the simulation, **(a)** for the time-uniform forcing runs and **(b)** for the time-varying forcing runs. **(c)** The time trajectory of hydrate inventory, Base (time-varying) vs. T0 (time-uniform).

Title Page

Abstract

Introduction

Conclusions

References

Tables

Figures

⏪

⏩

◀

▶

Back

Close

Full Screen / Esc

Printer-friendly Version

Interactive Discussion

Passive coastal margin deep sedimentary carbon and methane cycles

D. E. Archer et al.

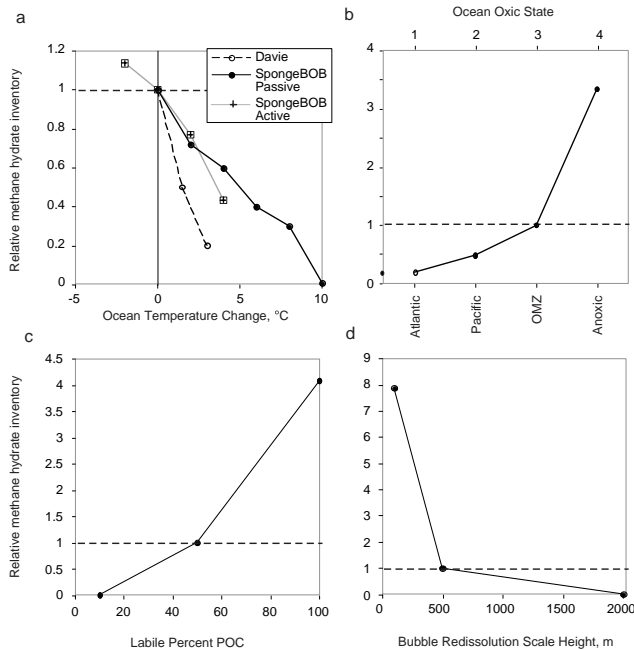


Fig. 17. Summary of model sensitivities. Y-axis is the hydrate inventory relative to the appropriate base case = 1. **(a)** Temperature, **(b)** ocean oxidic state (see Fig. 4), **(c)** percent labile fraction of depositing POC, and **(d)** migrating bubble redissolution scale height.

Title Page

Abstract Introduction

Conclusions References

Tables Figures

◀ ▶

◀ ▶

Back Close

Full Screen / Esc

Printer-friendly Version

Interactive Discussion

